Asian Journal of Chemistry; Vol. 33, No. 8 (2021), 1824-1830

ASIAN JOURNAL OF CHEMISTRY

https://doi.org/10.14233/ajchem.2021.23245

Swertia chirata Extract Synthesized Iron Oxide Nanoparticles as Corrosion Inhibitor for SS-316L in Hank's Solution

POOJA SHARMA[1], NISHANT BHARDWAJ[2] and VINEET KUMAR[1,*]

[1]Department of Biotechnology, School of Bioengineering and Biosciences, Lovely Professional University, Phagwara-144111, India
[2]Department of Chemistry, Lovely Professional University, Phagwara-144111, India

*Corresponding author: E-mail: vineetkumar22@gmail.com; vineet.21644@lpu.co.in

Received: 12 April 2021; *Accepted*: 20 May 2021; *Published online*: 26 July 2021; AJC-20434

Metallic implants are the artificial biomedical devices used to replace, repair or improve the functioning of damaged body organ or tissue. Corrosion of metallic component in the human body leads to the failure or improper functioning of the implant. This study focuses on the application of *Swertia chirata* extract synthesized iron oxide nanoparticles as corrosion inhibitor for stainless steel (SS) 316L in Hank's solution. Gravimetric method and electrochemical studied were used to analyze the corrosion inhibition property. SEM and AFM analyses confirmed the corrosion preventive effect of iron oxide nanoparticles on SS-316L surface. Further concentration dependent increase in inhibition efficiency was observed with maximum 80.3% corrosion inhibition at 100 ppm nanoparticles concentration from gravimetric analysis, which is well correlated with the electrochemical measurements. Therefore, iron oxide nanoparticles can be utilized as potent anticorrosive agent, which can protect the metal surface from further deterioration in harsh body environments.

Keywords: Iron oxide, SS-316L, Hank's solution, Biomedical implants, Anticorrosion, Electrochemical analysis.

INTRODUCTION

The advancement in healthcare technology and biological needs has increased the use of implants. The materials to be used as an implant is chosen on the basis of their biocompatibility and applicability [1]. Materials of metallic nature are highly employed for such purpose as they are efficient in tension loadings and are of high mechanical strength. Biomaterials or implants are used as stents for replacement of dental structures, knee and hip joints to name a few [2]. The SS-316L is used in implant devices like as prosthetics, stents, catheters, dental implants, plates for cranial or orthopedic fractures [3].

Corrosion is an important factor in selection and designing of metals to be used for such *in vivo* applications. The bio-implants are placed in various body parts and the type and concentration of body fluid present in that part can act as a corrosive environment [4]. The major problem associated with corrosion include local pain, infection and swelling or lack of adherence to the body tissue is corrosion. Many factors are associated with corrosion process in human body like chloride ions, pH or dissolved oxygen [5]. Loosening of implant or its failure occurs in some cases due to the electrochemical process occurring on the surface of material which leads to the leaching of ions from implant surface to the surrounding tissues. For the protection of metals and alloys from corrosion, inhibitors based on plant extracts have been used extensively [6]. Hank's solution is composed of many dissolved ions like sodium, potassium, calcium, chloride and bicarbonate that is present in whole body tissues. The chloride ions are well known for their aggressive behaviour towards metals. This oxygenated saline which is rich in electrolyte at human body (pH 7.4 at 37 ºC) facilitate the corrosion process after the implantation of metals in the body. The electrochemical reactions start at the tissue-implant interface due to the presence of these ions thus making the body environment harsh and prone to corrosion. Many studies have been reported on corrosion testing of materials in Hank's solution [7-9].

Iron oxide NPs have some unique properties like good stability in colloidal solutions, magnetic behaviour and good biocompatibility, which makes them suitable for various biomedical applications [10]. For the synthesis of nano-materials, green methods are generally applied now-a-days

because such methods offer various benefits like eco-friendly and more compatible nanomaterials for biomedical and pharmaceutical use [11]. To simulate the body fluid environment, Hank's solution has been used extensively to analyze the process and rate of corrosion of various body implants [12].

Swertia chirata belongs to the family Gentianaceae. It comes under the group of annual or perennial plants used as herb for their medicinal properties and grows at very high altitudes where sub temperate conditions are found in Himalayas. It contains various phytochemicals which includes amarogentin, the most bitter tasted compound along with swerchirin, swertiamarin, amarogentin and amaroswin [13]. This study focuses on the green synthesis of iron oxide nanoparticles from *Swertia chirata* and to investigate their anticorrosion properties on SS-316L.

EXPERIMENTAL

Plant extract preparation and iron oxide NPs synthesis: *Swertia chirata* dried stem was collected from Jalandhar, India. The identification and authentication were carried out by Botanical Survey of India. The plant material was ground to powder form. Then, 2 g powder was added in a flask containing 50 mL of double distilled water and boiled for 10 min. The mixture was cooled and centrifuged at 10,000 rpm for 10 min. The clear supernatant was used as plant extract for further studies.

Ferric chloride of high purity was purchased from Loba Chemical. The synthesis of nanoparticles was done by previously reported method [14,15]. Briefly, 1 mL of 10 mM ferric chloride solution was added to 1 mL of plant extract (1:1 ratio). The mixture was allowed to stand for 10 min and then centrifuged at 10,000 rpm for 10 min. The obtained NPs were washed thrice with ethanol and dried at room temperature, 25 ºC. The synthesized NPs were used for further studies [14-16].

Anticorrosive studies

Preparation of working sample of SS-316L and weight loss measurements: The elemental composition of used SS-316L was Fe (65.73%), Cr (17.54%), Mn (1.26%), Mo (2.43%), C (0.6%), P (0.018%), Ni (12.36%), S (0.017%) and Si (0. 58%). For the preparation of working electrode, SS-316L 316L specimen of 10 mm diameter and area 1 cm^2, were immersed in epoxy resin. Working electrode surface was abraded by using emery paper of 100, 320, 600, 800, 1000 and 1200 grades. The coupons of SS-316L of area 1 cm^2 were used for gravimetric method. The synthesized NPs were dispersed in the Hank's solution to obtain different working concentrations, 10, 25, 50, 75 and 100 ppm.

Weight loss tests were performed with 10 ppm, 25 ppm, 50 ppm, 75 ppm and 100 ppm of ron oxide NPs in Hank's solution at room temperature for 120 h. For the weight loss experiment SS-316L samples having an area of 1 cm^2 were used. The SS-316L samples were weighed and immersed in the test solution in the absence and presence of NPs for 120 h. After 120 h, the SS-316L samples were taken out from the test solution, rinsed with acetone, dried under nitrogen flow and weighed according to ASTM G 31 [17].

Adsorption study

Scanning electron microscopy: Scanning electron microscope (SEM, JEOL) was used for taking the surface micrograph of SS-316L. SEM images were captured for polished steel and steel samples immersed in corrosive media in the absence and presence of NPs.

Atomic force microscopic study: AFM was used for the surface investigation of SS-316L for the AFM study, the surface of SS-316L was cleaned using ultrapure water followed by acetone. Abraded SS-316L, SS-316L immersed in Hank's solution and SS-316L immersed in Hank's solution containing 100 ppm of iron oxide NPs were characterized using AFM.

Electrochemical measurements: Auto lab electrochemical workstation (Metrohm) with three-electrode electrochemical cell were used for electrochemical impedance spectroscopy and potentiodynamic polarization. The obtained Tafel polarization curves were recorded between -200 to +200 mV *versus* Ag/AgCl (3 M KCl) with scanning rate of 0.1 mV/s. The electrochemical measurements were conducted at 10 mV amplitude and 100 kHz to 0.01 Hz frequency [18-21]. The data obtained was calculated using CHI 760C electrochemical work station software.

RESULTS AND DISCUSSION

Weight loss measurements: Corrosion inhibition efficiency of iron oxide NPs was calculated for the surface of SS-316L in the presence of Hank's solution as corrosive medium. Corrosion rate of SS-316L in corrosive media containing different concentration of iron oxide NPs were calculated using eqn. 1:

$$C_R = \frac{K \times W}{A \times t \times \rho} \quad (1)$$

where, C_R is corrosion rate (mm $year^{-1}$), w is weight loss of SS-316L, t signifies the immersion time (h) of SS-316L, ρ is the density (7.86 g cm^{-3}) of the SS-316L as per the literature of ASTM and k is the corrosion constant (8.76×10^4).

The value of corrosion inhibition efficiency (IE) and surface coverage (θ) of iron oxide NPs was calculated using eqns. 2 and 3:

$$IE\ (\%) = \frac{C_R^o - C_R^i}{C_R^o} \times 100 \quad (2)$$

$$\theta = \frac{C_R^o - C_R^i}{C_R^o} \quad (3)$$

where, the corrosion rate of immersed SS-316L in corrosive media and in iron oxide NPs solution was mentioned by C_R^o and C_k^i, respectively. As the concentration of iron oxide NPs increases, the value of corrosion rate decreases thus leading to an increase in corrosion inhibition efficiency. The decrease in the of value of corrosion rate is due to adsorption of iron oxide NPs on the surface of SS-316L. Maximum 80.30 % corrosion inhibition efficiency was recorded using 100 ppm iron oxide NPs. The values for main parameters are mentioned in Table-1.

Adsorption isotherm study: Langmuir adsorption isotherm was used for explaining the adsorption behaviour of iron oxide NPs on SS-316L surface. The concentration of iron oxide NPs used and the value of surface coverage which iron oxide NPs provided to SS-316L were the main component of this study. Graph between C/θ and C was recorded as shown in Fig. 1.

$$\frac{C}{\theta} = \frac{1}{K_{ads}} + C \quad (4)$$

where, K_{ads} is used for equilibrium adsorption constant. The linear correlation coefficients (0.9969) was almost equal to 1, which confirmed that the adsorption of iron oxide NPs obey Langmuir adsorption isotherm and the data is shown in Table-1.

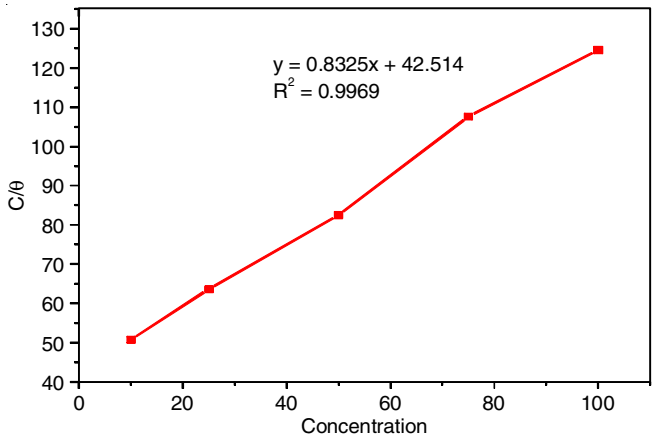

Fig. 1. Adsorption isotherm of iron oxide NPs on the SS-316L surface

Surface investigation

Scanning electron microscope: The surface morphology of SS-316L in Hank's solution was analyzed using SEM images of abraded SS-316L, SS-316L sample immersed in Hank's solution and SS-316L sample immersed in Hank's solution with 100 ppm of iron oxide NPs are shown in Fig. 2a-c, respectively. It is clear from the SEM analysis that the SS-316L sample immersed in Hank's solution has rough and corroded surface while the surface of SS-316L sample immersed in iron oxide NPs containing Hank's solution appeared smooth due to corrosion inhibition activity of iron oxide NPs [22-24].

Atomic force microscopic study: The AFM images of polished and clean, SS-316L immersed in Hank's solution and Hank's solution with 100 ppm of iron oxide NPs are shown in Fig. 3a-c, respectively. The surface roughness value for SS-316L sample, which is polished and SS-316L sample immersed in Hank's solution were 29 nm and 880 nm, respectively. Increase in surface roughness of after immersion in corrosive media indicated the level of corrosion as the abraded SS-316L samples surface loses smoothness as a result of corrosion [25]. SS-316L samples immersed in Hank's solution with 100 ppm of iron oxide NPs possessed comparatively lower 423 nm surface roughness as a result of corrosion inhibitory activity of NPs. More detailed AFM analysis revealed that the iron oxide NPs tend to aggregate over the surface of SS-316L. The cluster size increases up to 150-200 nm. The clustering is helpful for corrosion inhibition properties as the materials try to stick to the SS-316L surface. This is due to neutral zeta potential of the iron oxide NPs that help NPs to aggregate and

TABLE-1
WEIGHT LOSS MEASUREMENTS FOR SS-316L IN HANK'S SOLUTION WITHOUT AND WITH DIFFERENT CONCENTRATIONS OF NPs

Concentration (C)	Corrosion rate, C_R (mm y^{-1})	Inhibition efficiency (%)	Surface coverage (θ)	C/θ
Hank's solution	0.00066	–	–	–
Hank's solution + 10 ppm iron oxide NPs	0.00053	19.69	0.1969	50.78
Hank's solution + 25 ppm iron oxide NPs	0.00040	39.30	0.3930	63.61
Hank's solution + 50 ppm iron oxide NPs	0.00026	60.61	0.6061	82.49
Hank's solution + 75 ppm iron oxide NPs	0.00020	69.69	0.6969	107.61
Hank's solution + 100 ppm iron oxide NPs	0.00013	80.30	0.8030	124.53

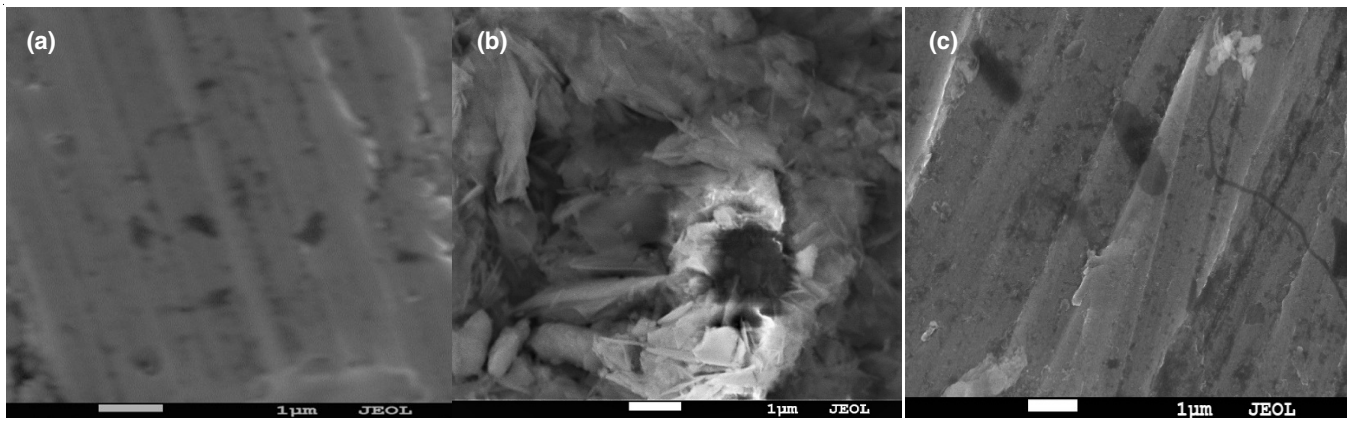

Fig. 2. SEM images of (a) polished SS-316L surface, (b) SS-316L immersed in Hank's solution and (c) SS-316L immersed in Hank's solution with 100 ppm of NPs

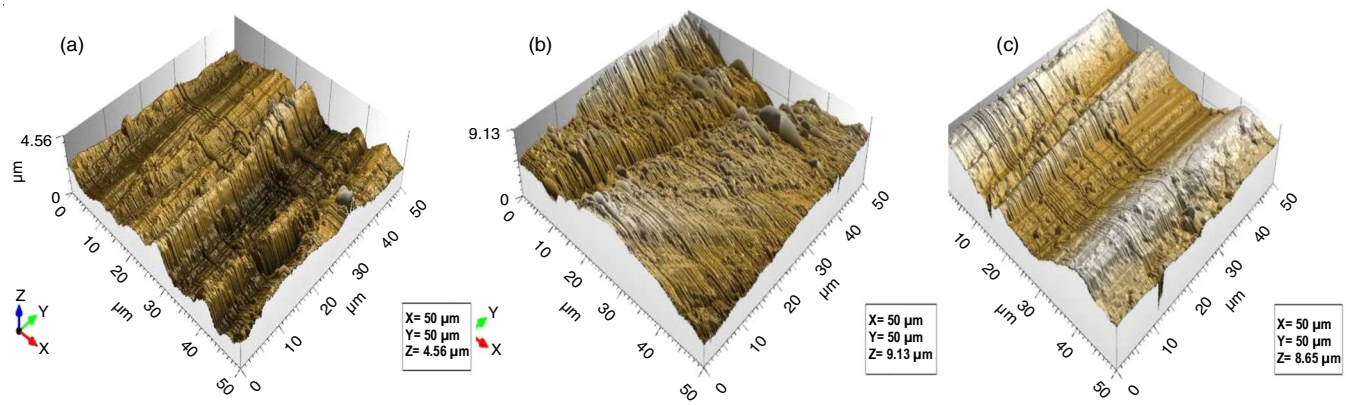

Fig. 3. AFM images of (a) polished SS-316L surface, (b) SS-316L immersed in Hank's solution (c) SS-316L immersed in Hank's solution with 100 ppm of NPs

the phytochemicals present on the surface of iron oxide NPs that have binding to SS-316L surface [26,27].

UV visible study: The UV-visible spectra of 100 ppm iron oxide NPs dissolved in Hank's solution, before and after immersion of SS-316L specimen is shown in Fig. 4. The solution in which SS-316L samples were not immersed show higher peak absorbance spectra with respect to the solution in which SS-316L samples were immersed in which there is shift in the value of adsorption maxima. The shift or lower adsorption spectra of SS-316L sample immersed in iron oxide NPs containing solution indicated the adsorption of NPs present in the solution on SS-316L surface and the formation of bonds with the Fe^{2+} particles from SS-316L surface and the NPs [28]. Therefore, when SS-316L specimen is immersed in the iron oxide NPs containing Hank's solution, some of the NPs from the solution get adsorbed on the SS-316L surface by the process of protonation of heteroatoms of NP's surface and their electrostatic interactions with the SS-316L surface and it is proposed that the NPs get adsorbed on the SS-316L surface and make complexes with the surface atoms of substrate surface thus by forming a protective layer to slow down the corrosion process and act as good corrosion inhibitors [28].

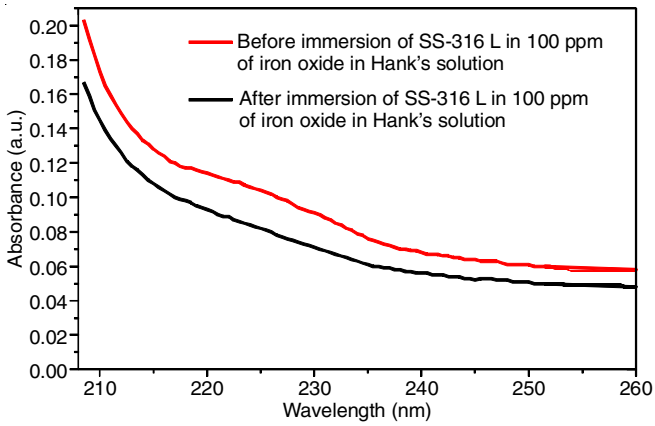

Fig. 4. UV-visible spectra of 100 ppm iron oxide NPs before and after immersion of SS-316L specimen in Hank's solution

Electrochemical study

Potentiodynamic polarization: The working electrode of SS-316L were immersed in Hank's solution with 10, 25, 50, 75 and 100 ppm of the iron oxide NPs solution. There was decrease in current densities with increase in iron oxide NPs concentration from 10 to 100 ppm. The value of corrosion inhibition efficiency was calculated using eqn. 5:

$$IE\ (\%) = \frac{I^{o}_{corr} - I^{i}_{corr}}{I^{o}_{corr}} \times 100 \quad (5)$$

where I^{o}_{corr} and I^{i}_{corr} were used for corrosion current density of Hank's solution and iron oxide NPs suspension as inhibitor. The polarization curve is shown in Fig. 5a. As the amount of iron oxide NPs increases in the corrosive media, the value of corrosion current density decreases, which designate the increase in corrosion inhibition efficiency [29-31]. The value of E_{corr} was found to be between 30-35 mV. It has been reported earlier that if the maximum shift in the value of corrosion potential (E_{corr}) from the corrosive solution is within the range of 85 mV the inhibition is of mixed (anodic or cathodic inhibition) type. Iron oxide NPs have shown mixed type of inhibition behaviour [32-34]. The 78.98% corrosion inhibition efficiency was recorded at concentration of 100 ppm iron oxide NPs in Hank's solution as mentioned in Table-2.

Electrochemical impedance spectroscopy: Working electrode of SS-316L samples was immersed in Hank's solution containing 10 to 100 ppm iron oxide NPs. Nyquist plot revealed that there is increase in the value of charge transfer resistance with increase in concentration of iron oxide NPs (Fig. 5b) [35-37]. This designated increase in the corrosion inhibition efficiency with increase in concentration of iron oxide NPs. Corrosion inhibition efficiency were calculated using eqn. 6:

$$IE\ (\%) = \frac{R_{ct} - R^{o}_{ct}}{R_{ct}} \times 100 \quad (6)$$

where, R_{ct} and R^{o}_{ct} designates charge transfer resistance of different concentrations of iron oxide NPs and Hank's solution, respectively. A maximum 76.83 % corrosion inhibition efficiency was obtained as clear from Table-3. Layer formation was evident from increase in the R_{ct} value with increases in iron oxide NPs concentration. The Bode plot shown in Fig. 6a, support the concept of iron oxide NPs adsorption on the SS-316L surface [38]. This process leads to efficient anti-corrosive property of iron oxide NPs. The phase angles graph is shown

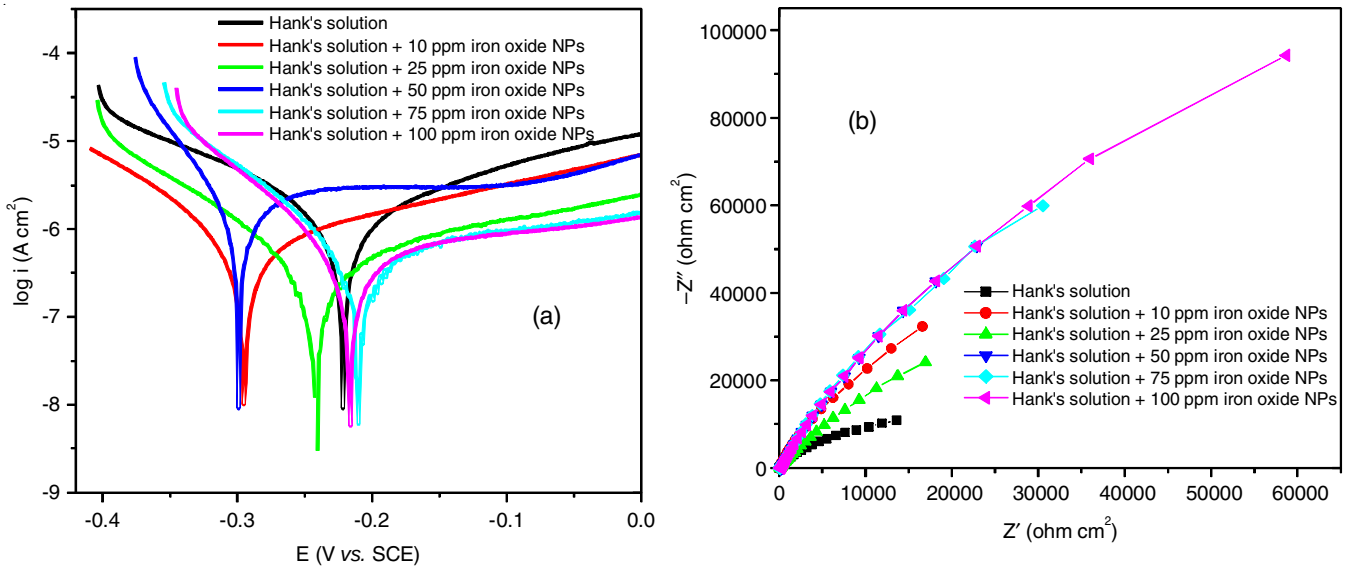

Fig. 5. Electrochemical studies on SS-316L surface with iron oxide NPs (a) Tafel plot with different concentrations of iron oxide NPs (b) Nyquist plot with different concentrations of iron oxide NPs

TABLE-2
POLARIZATION PARAMETERS FOR SS-316L IN HANK'S SOLUTION WITHOUT AND WITH DIFFERENT CONCENTRATIONS OF Ns

Concentration	Corrosion current density, i_{corr} (A cm^{-2}) × 10^{-7}	Corrosion inhibition efficiency (%)
Hank's solution	8.71	
Hank's solution + 10 ppm iron oxide NPs	7.10	18.48
Hank's solution + 25 ppm iron oxide NPs	6.85	21.35
Hank's solution + 50 ppm iron oxide NPs	5.11	41.33
Hank's solution + 75 ppm iron oxide NPs	3.84	55.91
Hank's solution + 100 ppm iron oxide NPs	1.83	78.98

in Fig. 6b and it can be observed that the values obtained in the presence of inhibitors has shown the process of charge transfer resistance which started on the interface between electrode and electrolyte [39]. The phase angle values has shown that with increase in iron oxide NPs concentration, there was good inhibition due to the adsorption of particles on the surface of SS-316L and a protective film was formed as indicated by the data. The increment in the values of phase angle in the presence of NPs can be attribute to a decrease in the capacitance at the surface of SS-316L which makes the SS-316L surface less prone to dissolution in the presence of corrosive media [40]. Moreover, for the representation of reaction at

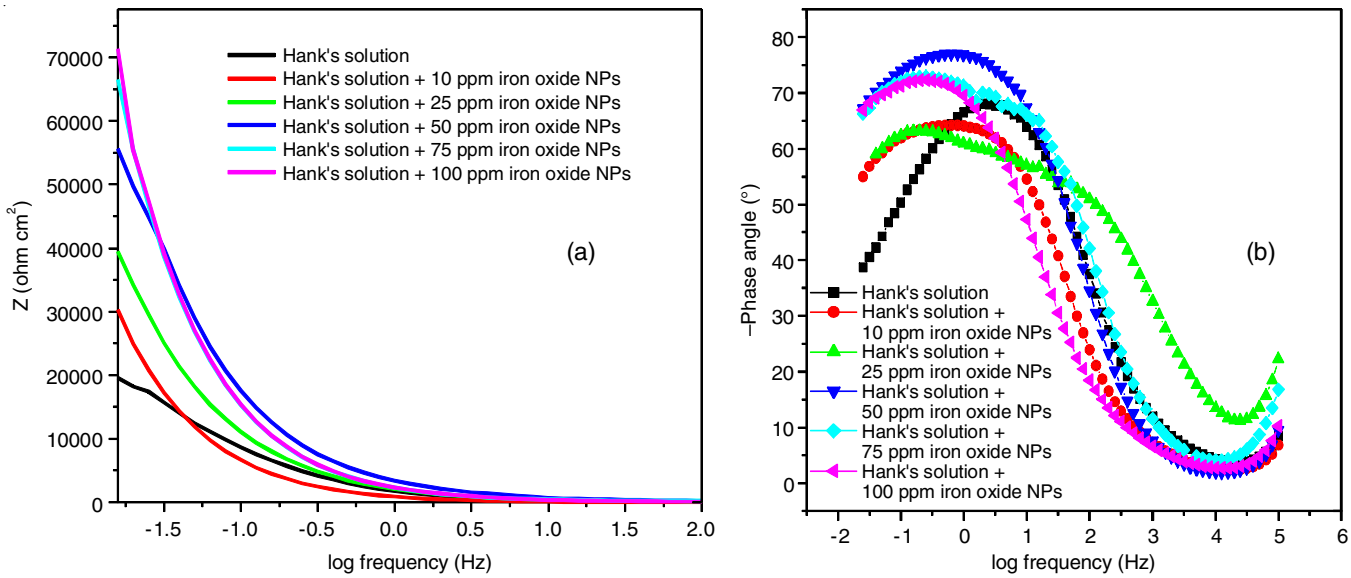

Fig. 6. (a) Bode plot with different concentrations of iron oxide NPs and (b) Phase angle plot with different concentrations of iron oxide NPs

TABLE-3
ELECTROCHEMICAL IMPEDANCE PARAMETERS FOR SS-316L IN HANK'S SOLUTION WITHOUT AND WITH DIFFERENT CONCENTRATIONS OF NPs

Concentration	Charge transfer resistance (Ω cm^{-2})	Corrosion inhibition efficiency (%)
Hank's solution	13588.78	–
Hank's solution + 10 ppm iron oxide NPs	16567.93	17.98
Hank's solution + 25 ppm iron oxide NPs	16884.19	19.51
Hank's solution + 50 ppm iron oxide NPs	22880.33	40.60
Hank's solution + 75 ppm iron oxide NPs	30479.31	55.41
Hank's solution + 100 ppm iron oxide NPs	58668.96	76.83

electrode and electrolyte interface, an equivalent circuit was also fitted with ZSimpWimp V3.20 which is shown in Fig. 7. The proposed mechanism for the corrosion inhibition behaviour of iron oxide NPs on SS-316L surface is shown in Fig. 8.

The findings of electrochemical impedance and potentiodynamic polarization collectively proved the corrosion inhibitor efficacy of NPs. The real time kinetics was obtained by measuring PDP as it gives wide range polarization where possibility of occurrence of irreversible change during the process of measurement was present while the data of EIS was taken at OCP which helps in getting the measured values for interfacial resistance occurring at the interface of electrode and electrolyte [41,42]. The results obtained from EIS was in good agreement with the PDP. The PDP measurements provide real time kinetics of the electrochemical processes (polarization at wide range of potential with a possible irreversible change occurring due to the measuring process) and EIS data was usually obtained at the OCP and provide measured values of the overall interfacial resistance at the electrode-electrolyte interface [43,44].

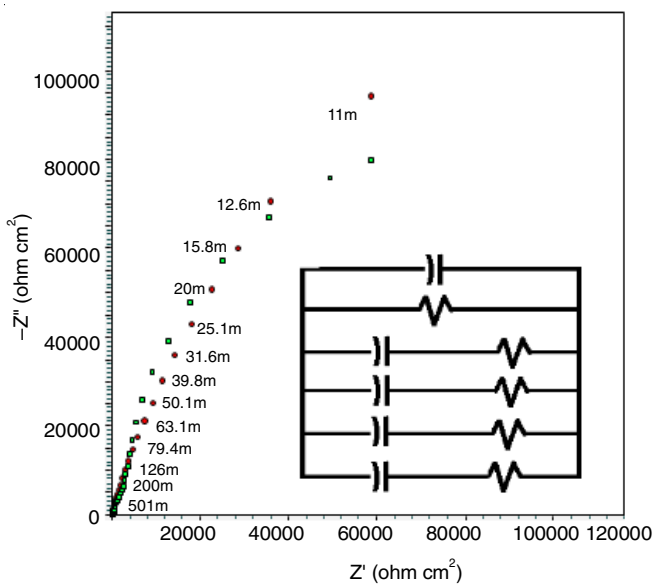

Fig. 7. Electrochemical curve fitting with circuit of 100 ppm iron oxide NPs

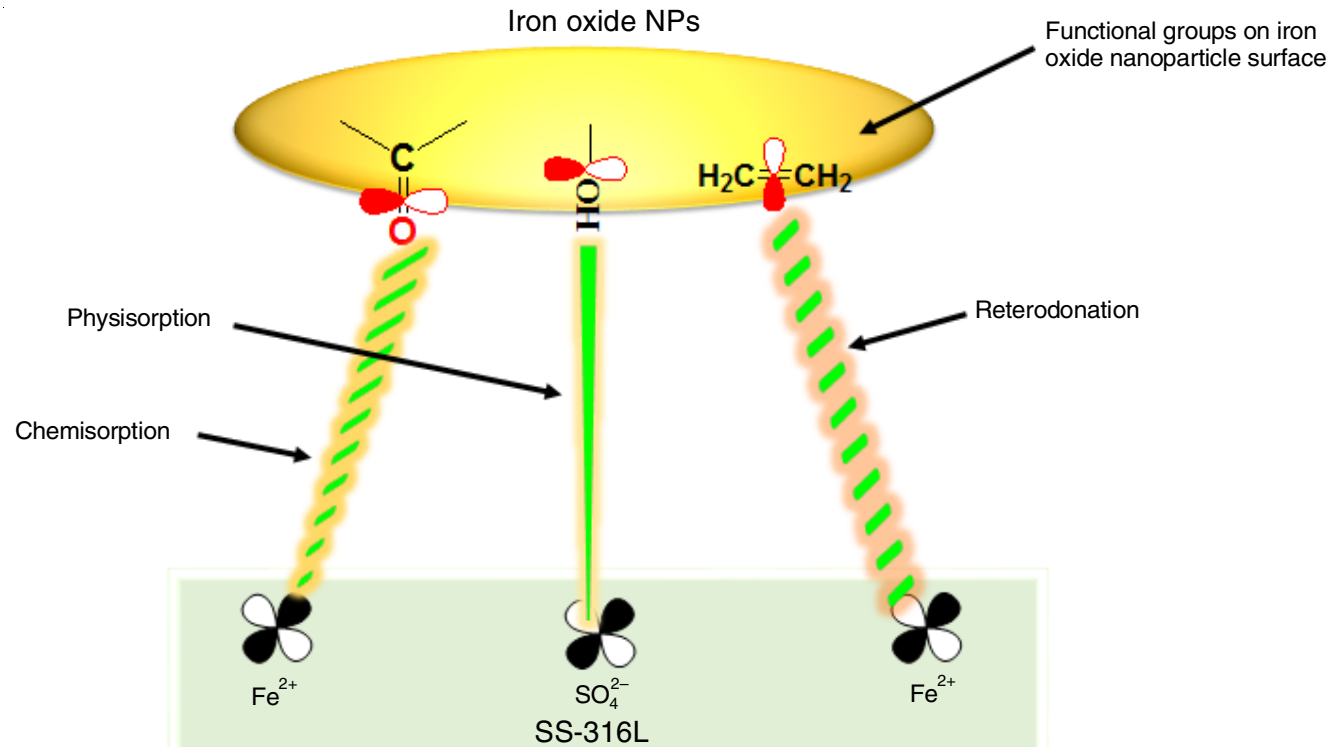

Fig. 8. Proposed mechanism of inhibition of iron oxide NPs on the surface of SS-316L

Conclusion

The anticorrosion studies, gravimetric analysis, electrochemical test and surface investigation studies proved the corrosion inhibition efficiency of *Swertia chirata* extract prepared iron oxide NPs against SS-316L in Hank' solution. The increase in the concentration of NPs was found to have improvement in corrosion inhibition efficiency. The NPs follow Langmuir adsorption isotherm that indicated monolayer formation on the surface of SS-316L. Furthermore, the potentiodynamic polarization studies proved that the NPs show mixed type of corrosion inhibition in Hank's solution. The surface studies conducted using SEM and AFM confirmed the corrosion inhibition behaviour of nano-particles. Therefore, iron oxide NPs has potential to act as corrosion inhibitor for SS-316L used for biomedical purpose, SS-316L in Hank's solution mimicking *in vivo* condition.

ACKNOWLEDGEMENTS

PS, NB and VK are thankful to Central Instrumental Facility, Lovely Professional University for providing the necessary instrument facilities. Authors are also thankful to Guru Nanak Dev University Amritsar for AFM facility.

CONFLICT OF INTEREST

The authors declare that there is no conflict of interests regarding the publication of this article.

REFERENCES

1. N. Eliaz, *Materials*, **12**, 407 (2019); https://doi.org/10.3390/ma12030407
2. M.A. Hussein, A.S. Mohammed and N. Al-Aqeeli, *Materials*, **8**, 2749 (2015); https://doi.org/10.3390/ma8052749
3. K. Prasad, O. Bazaka, M. Chua, M. Rochford, L. Fedrick, J. Spoor, R. Symes, M. Tieppo, C. Collins, A. Cao, D. Markwell, K.K. Ostrikov and K. Bazaka, *Materials*, **10**, 884 (2017); https://doi.org/10.3390/ma10080884
4. N.S. Manam, W.S.W. Harun, D.N.A. Shri, S.A.C. Ghani, T. Kurniawan, M.H. Ismail and M.H.I. Ibrahim, *J. Alloys Compd.*, **701**, 698 (2017); https://doi.org/10.1016/j.jallcom.2017.01.196
5. G. Manivasagam, D. Dhinasekaran and A. Rajamanickam, *Recent Pat. Corros. Sci.*, **2**, 40 (2010); https://doi.org/10.2174/1877610801002010040
6. N. Bhardwaj, P. Sharma and V. Kumar, *Corros. Rev.*, **39**, 27 (2021); https://doi.org/10.1515/corrrev-2020-0046.
7. J. Tkacz, K. Slouková, J. Minda, J. Drábiková, S. Fintová, P. Dolezal and J. Wasserbauer, *Metals*, **7**, 465 (2017); https://doi.org/10.3390/met7110465
8. S.B. Arya, A. Bhattacharjee and M. Roy, *Mater. Corros.*, **69**, 1025 (2018); https://doi.org/10.1002/maco.201709894
9. X. Niu, H. Shen, J. Fu, J. Yan and Y. Wang, *Corros. Sci.*, **157**, 284 (2019); https://doi.org/10.1016/j.corsci.2019.05.026
10. N.V. Srikanth Vallabani and S. Singh, *3 Biotech*., **8**, 279 (2018); https://doi.org/10.1007/s13205-018-1286-z
11. S. Kanagasubbulakshmi and K. Kadirvelu, *Defence Life Sci. J.*, **2**, 422 (2017); https://doi.org/10.14429/dlsj.2.12277
12. B. Sivakumar, L.C. Pathak and R. Singh, *Appl. Surf. Sci.*, **401**, 385 (2017); https://doi.org/10.1016/j.apsusc.2017.01.033
13. V. Kumar and J. Van Staden, *Front. Pharmacol.*, **6**, 308 (2016); https://doi.org/10.3389/fphar.2015.00308
14. V. Kumar and S.K. Yadav, *J. Chem. Technol. Biotechnol.*, **84**, 151 (2009); https://doi.org/10.1002/jctb.2023
15. V. Kumar, S.C. Yadav and S.K. Yadav, *J. Chem. Technol. Biotechnol.*, **85**, 1301 (2010); https://doi.org/10.1002/jctb.2427
16. V. Kumar, K. Singh, S. Panwar and S.K. Mehta, *Int. Nano Lett.*, **7**, 123 (2017); https://doi.org/10.1007/s40089-017-0205-3
17. A.C. Richard, Laboratory Corrosion Testing of Medical Implants, ASM International, Newyark, Delaware, USA (2003).
18. ASTM F2129-17b, Standard Test Method for Conducting Cyclic Potentiodynamic Polarization Measurements to Determine the Corrosion Susceptibility of Small Implant Devices, ASTM International, West Conshohocken, PA (2017).
19. L. Zhang, X. Tong, J. Lin, Y. Li and C. Wen, *Corros. Sci.*, **169**, 108602 (2020); https://doi.org/10.1016/j.corsci.2020.108602
20. D. Mei, C. Wang, S.V. Lamaka and M.L. Zheludkevich, *J. Magnesium Alloys*, **9**, 805 (2021); https://doi.org/10.1016/j.jma.2020.07.002
21. J. Tkacz, K. Slouková, J. Minda, J. Drábiková, S. Fintová, P. Dolezal and J. Wasserbauer, *Metals*, **7**, 465 (2017); https://doi.org/10.3390/met7110465
22. J. Tkacz, K. Slouková, J. Minda, J. Drábiková, S. Fintová, P. Dolezal and J. Wasserbauer, *Koroze a Ochrana Mater.*, **60**, 101 (2016); https://doi.org/10.1515/kom-2016-0016
23. E. Tamam and I. Turkyilmaz, *J. Oral Implantol.*, **40**, 153 (2014); https://doi.org/10.1563/AAID-JOI-D-11-00083
24. R. Ambat, N.N. Aung and W. Zhou, *J. Appl. Electrochem.*, **30**, 865 (2000); https://doi.org/10.1023/A:1004011916609
25. H. Altun and S. Sen, *Mater. Des.*, **25**, 637 (2004); https://doi.org/10.1016/j.matdes.2004.02.002
26. L.Y. Wu, Y.L. Kuo, K.H. Chang, T.H. Chen, C.Y. Cheng, Y.S. Liu and C. Huang, *Surf. Interface Anal.*, **51**, 993 (2019); https://doi.org/10.1002/sia.6684
27. M.C. Merino, A. Pardo, R. Arrabal, S. Merino, P. Casajus and M. Mohedano, *Corros. Sci.*, **52**, 1696 (2010); https://doi.org/10.1016/j.corsci.2010.01.020
28. A. Dehghani, G. Bahlakeh, B. Ramezanzadeh and M. Ramezanzadeh, *Constr. Build. Mater.*, **245**, 118464 (2020); https://doi.org/10.1016/j.conbuildmat.2020.118464
29. S. Shetty, J. Nayak and N. Shetty, *J. Magnes. Alloys*, **3**, 258 (2015); https://doi.org/10.1016/j.jma.2015.07.004
30. G.F. Vander Voort, Metallography, Principles and Practice, ASM International: Materials Park, OH, USA, Ed. 1, pp. 1-752 (1999).
31. J. Tkacz, J. Minda, S. Fintová and J. Wasserbauer, *Materials*, **9**, 925 (2016); https://doi.org/10.3390/ma9110925
32. S.E. Harandi, P.C. Banerjee, C.D. Easton and R.K. Singh Raman, *Mater. Sci. Eng. C*, **80**, 335 (2017); https://doi.org/10.1016/j.msec.2017.06.002
33. O. Igwe and F. Nwamezie, *Chem. Int.*, **4**, 60 (2018).
34. T. Mengistie, A. Alemu and A. Mekonnen, *Chem. Int.*, **4**, 130 (2018).
35. N. Eliaz and E. Gileadi, Physical Electrochemistry: Fundamentals, Techniques and Applications. John Wiley & Sons (2019).
36. Y. Zhu, G. Wu, Y.H. Zhang and Q. Zhao, *Appl. Surf. Sci.*, **257**, 6129 (2011); https://doi.org/10.1016/j.apsusc.2011.02.017
37. Y. Song, D. Shan, R. Chen, F. Zhang and E.-H. Han, *Mater. Sci. Eng. C*, **29**, 1039 (2009); https://doi.org/10.1016/j.msec.2008.08.026
38. D.H. Abdeen, M.A. Atieh and B. Merzougui, *Materials*, **14**, 119 (2020); https://doi.org/10.3390/ma14010119
39. A. Pardo, M.C. Merino, A.E. Coy, R. Arrabal, F. Viejo and E. Matykina, *Corros. Sci.*, **50**, 823 (2008); https://doi.org/10.1016/j.corsci.2007.11.005
40. I. Milosan, M. Florescu, D. Cristea, I. Voiculescu, M.A. Pop, I. Cañadas, J. Rodriguez, C.A. Bogatu and T. Bedo, *Materials*, **13**, 581 (2020); https://doi.org/10.3390/ma13030581
41. M. Alahiane, R. Oukhrib, Y.A. Albrimi, H.A. Oualid, H. Bourzi, R.A. Akbour, A. Assabbane, A. Nahlé and M. Hamdani, *RSC Adv.*, **10**, 41137 (2020); https://doi.org/10.1039/D0RA06742C
42. E. Ituen, L. Yuanhua, A. Singh and R. Li, *J. King Saud Univ. Eng. Sci.*, (2020); https://doi.org/10.1016/j.jksues.2020.05.005
43. S. Feliu Jr. and I. Llorente, *Appl. Surf. Sci.*, **347**, 736 (2015); https://doi.org/10.1016/j.apsusc.2015.04.189.
44. R. Walter and M.B. Kannan, *Mater. Des.*, **32**, 2350 (2011); https://doi.org/10.1016/j.matdes.2010.12.016